Title

COHERENCE IN ELECTRONICALLY EXCITED DIMERS. III. THE OBSERVATION OF COHERENCE IN DIMERS USING OPTICALLY DETECTED ELECTRON SPIN RESONANCE IN ZERO FIELD AND ITS RELATIONSHIP TO COHERENCE IN ONE-DIMENSIONAL EXCITONS

Authors

Zewail, A.H.
Harris, C.B.

Publication Date

1974-08-14

Submitted to [redacted] Physical Review B

LBL-3139
Preprint c.2

COHERENCE IN ELECTRONICALLY EXCITED DIMERS. III. THE OBSERVATION OF COHERENCE IN DIMERS USING OPTICALLY DETECTED ELECTRON SPIN RESONANCE IN ZERO FIELD AND ITS RELATIONSHIP TO COHERENCE IN ONE-DIMENSIONAL EXCITONS.

A. H. Zewail and C. B. Harris

August 14, 1974

Prepared for the U. S. Atomic Energy Commission
under Contract W-7405-ENG-48

DISCLAIMER

COHERENCE IN ELECTRONICALLY EXCITED DIMERS. III. THE OBSERVATION OF COHERENCE IN DIMERS USING OPTICALLY DETECTED ELECTRON SPIN RESONANCE IN ZERO FIELD AND ITS RELATIONSHIP TO COHERENCE IN ONE-DIMENSIONAL EXCITONS.

A. H. Zewail and C. B. Harris*

Inorganic Materials Research Division, Lawrence Berkeley Laboratory;
and Department of Chemistry; University of California
Berkeley, California 94720

*Alfred P. Sloan Fellow

ABSTRACT

The observation of coherent dimers in their excited triplet state is reported for a molecular crystal of 1,2,4,5-tetrachlorobenzene at low temperatures (below 4.2K). Utilizing the theory developed in our previous paper, the coherence time (10^{-6} sec) and the anisotropy of the resonance interactions in the excited state were established. The identification of the dimer as translationally equivalent, from the zero field optically detected magnetic resonance spectra, establishes the effective dispersion for the triplet exciton band of the neat crystal. Moreover, the magnitude of the resonance transfer time was shown to be much less than the coherence time: the dimer is coherent for a period of 10^5 times that associated with the stochastic limit.

I. INTRODUCTION

The growing interest in studying energy transport in insulators is surely evidence of the many unknown and interesting questions which pertain to this problem. A large effort was devoted to establish whether or not the energy migration is coherent or incoherent. In the coherent description[1-5] of energy migration, excitons are described by a group velocity, $V_g(k)$, and hence the individual k states are characterized by a coherence length, $\ell(k)$, and a coherence time, $\tau(k)$. The magnitude of $\ell(k)$ is determined by the nature of scattering centers in crystals. Moreover, the propagation of the exciton is determined by many radiative and non-radiative processes such as trapping,[6] surface quenching,[7] exciton-exciton interactions[8] and exciton-phonon coupling.[1] The influence of the latter on the exciton properties was investigated both by optical[9] and magnetic resonance[10,5] spectroscopy and different models have been adopted for the coupling. The linear exciton-phonon interaction treatment was given by Holstein[11] in discussing self-trapping of polarons and by Silbey[12] in treating the coupling in the one-dimensional case, whereas the quadratic exciton-phonon coupling was developed by Munn and Siebrand.[13] Recently the manifestations of the coupling in the magnetic spectra of excitons were shown[14] to be sensitive to the temperature and the exciton band width.

The extent to which this coupling alters the stationary and non-stationary properties of the band depends on the nature of the matrix elements which connect the exciton and phonon states. It is therefore

important to establish the dimensionality of the interactions as well as the scattering cross-sections.

A dimer is a two-molecule chain and therefore must have a direct relationship to the parent infinite-molecule chain (exciton). Hence, the physics governing the scattering processes and the anisotropy of the interactions are interrelated. In the previous paper[15] we have shown that low-temperature electron spin resonance in zero field is a suitable probe for studying the dynamics of energy transfer in dimer and exciton states. The salient features of that paper are: (1) The magnetic properties of translationally equivalent and translationally inequivalent dimers in their triplet states depend on the magnitude of the resonance interactions, and the local symmetry of the dimer and spin-orbital anisotropy determines the induced differences in the Larmor frequencies of $\psi(+)$ and $\psi(-)$ states. (2) The microwave absorption and dispersion in dimers are directly related to the microwave absorption and dispersion of triplet Frenkel excitons. Hence the dimensionality of the interactions can be established from the zero field EPR spectra. (3) The microwave absorption in dimer states depends on both the magnitude of the intermolecular interactions and the exciton-phonon coupling matrix elements which in turn determine the limit of spin exchange, slow, intermediate and fast. Hence coherence in the excited states of dimers and excitons can be established. Finally (4) the coherent properties of dimers depend on the statistics governing the scattering processes which may or may not lead into thermal equilibrium (Boltzmann distribution) and they are related to coherence in exciton states of molecular solids.

In this paper we present the following. (a) Coherence is clearly demonstrated in electronically excited dimers of 1,2,4,5-tetrachlorobenzene crystal at low temperatures, which to the best of our knowledge has not been established unequivocally before. (b) The optical detection of magnetic resonances in dimers establishes the dimensionality of the triplet exciton band which has been reported[5] from completely different measurements, namely the exciton zero field EPR transitions. Thus the experiments on dimers offer a way of measuring triplet exciton properties without going through the pain of getting exciton emission from many molecular crystals of interest, where trapping by impurities or dislocations is efficient. Finally, (c) the coherence time is proven to be approximately 10^5 times that of the stochastic limit, and also that it is related to the coherence time in the exciton band states.

II. EXPERIMENTAL

(A) The Optical Detection of Magnetic Resonance in Zero Applied Magnetic Field.

The basic arrangements for the zero field spectrometer are the same as those published[16] before for the optical detection of resonances from phosphorescent states. However, in our own experiments and others similar, where the signal-to-noise ratio is crucial in establishing some spectral features, the photon-flux must be maximized. Figure 1 shows the experimental setup for the detection of EPR transitions.

A single crystal was cut to fit inside a helical slow-wave structure matched to a 50 Ω rigid coaxial line. The whole assembly was immersed

in a liquid helium Dewar which could be pumped to temperatures between 1.3K and 2.1K, depending upon the specific experiment. The light from a PEK 100-W mercury-xenon lamp, whose arc gap is comparable with the crystal size so optimum illumination could be achieved, was collimated and filtered by a Schott interference filter whose peak is centered at approximately 2800 Å. The phosphorescence was collected at right angle to the exciting light, so the amount of light scattering was minimal, and focused onto the slit of a Czerny-Turner Jarrell-Ash (3/4 meter) spectrometer by a set of laser-mounted lenses. The output of the monochromator was focused on the photomultiplier, EMI 6256S, with a cooled (-20°C) housing to depress the dark current. The cathode of the photomultiplier was held at a negative voltage by a constant-voltage Fluke (415 B) power supply while the anode was connected either to a digital voltmeter (Preston Scientific Model 723A) or a Keithley Model 610 CR electrometer through a variable load resistor.

For the optimum conditions the following procedure was utilized. The grating of the spectrometer was placed at the desired wavelength and the phosphorescence intensity was displayed as a voltage on the digital voltmeter. The iris of the lamp was then narrowed to a point of illumination on the crystal, inside the helix, which was roughly the point of maximum rf field. The phosphorescence was maximized by focusing the output emission from the crystal on the slit. Finally, the full output flux of the lamp was utilized, and the output of the photomultiplier was fed into a PAR Model HR-8 lock-in amplifier with a load resistance.

The microwaves were obtained from a Hewlett-Packard sweep oscillator (Model 8690 B) equipped with an external assembly which permitted the

internal sweep circuit of the oscillator to be switched between external capacitors to obtain a sweep time as long as one hour with a sweep rate of 0.025 MHz per sec to provide higher RC (30-100 sec) time constants on the lock-in. The different microwave frequencies were obtained from different plug-in units which covered various bands, and the frequency was measured with a HP Model 5245 L electronic counter. Amplitude modulation of the microwaves was used in these experiments, and for good isolation two HP Model 33124 A PIN diodes in series giving a modulation depth of at least 60 dB were utilized. These switching devices (rise time of ≈10 nsec) were driven by a transistor-transistor LOGIC integrated device which gives the required amount of current in connection with a fast/slow LOGIC interface. The output from the oscillator was fed into two isolators and then to the PIN diodes which were switched on and off at the desired modulation frequency using a square-wave generator (Exact Electronics Type 255) which was also connected to the reference channel of the lock-in amplifier. The microwaves were then fed into a 20 watt TWT amplifier, whose output was filtered, isolated and then terminated in the coaxial line. Two directional couplers were used in this arrangement: one received the microwave field from the oscillator and split -10 dB of the total output into the counter or oscilloscope (Tektronix Model Type 454) while the rest of the power went to a number of attenuators (Narda #768) in series to adjust the desired level of microwave power, and then to the PIN diodes. The other directional coupler was used before the input to the coaxial line, so the total power output could be measured by a HP Model 431 A power meter. Finally, the output of the lock-in amplifier drove the Y-axis

of a Hewlett-Packard Model 7004 B X-Y recorder while the X-axis was driven by the ramp voltage from the sweep oscillator. For the recording of phosphorescence spectra, the output of the electrometer was fed into a strip chart recorder (HP Model 7100B).

(B) Crystal Preparations and the Phosphorescence Spectra.

The starting materials,[17] 1,2,4,5-tetrachlorobenzene-h_2 (H_2) and 1,2,4,5=tetrachlorobenzene-d_2 (D_2), were extensively zone-refined, 100 passes at approximately 3 cm per hour. The isotopically mixed single crystals were grown from the melt by standard Bridgman techniques. The compositions of these crystals were determined by mass spectroscopy. Table I contains the percentage composition of the three samples used in this work.

The single crystals were mounted inside the helix affixed to a section of the coaxial cable. After the crystal was cooled to 1.3K by pumping on the liquid helium with three Kenney Model KTC-21 vacuum pumps in parallel, the excited species were generated and the phosphorescence spectrum was recorded on a strip chart recorder. The temperature was obtained by measuring the vapor pressure of helium above the crystal, using ALPHATRON (NRC type 530) vacuum gauge.

III. RESULTS

(A) The Emission Spectra.

The unpolarized phosphorescence spectra of the isotopically mixed 1,2,4,5-tetrachlorobenzene (TCB) crystals show the emission of H_2, HD and D_2. The relative intensities are very sensitive to both the temperature

of the bath and the concentration of the guest. This, in fact, is the result of the communication[4] between the traps below the D_2 exciton band, as discussed before.[18] Figure 2 shows the emission spectra for three different concentrations of H_2 used in these experiments. The energy distance of HD (11 cm^{-1}) is almost half the distance of H_2 from the D_2 band. At higher guest concentration, the aggregation of the isolated molecules is expected to be more effective. Thus the emission spectra will display the phosphorescence of the different clusters (monomers, dimers, ... etc.), as shown in 1,4-dibromonaphthalene mixed crystals,[19] only if 2β is larger than the linewidth at half height. Given the halfwidth of the 0,0 emission of H_2 (ca.2 cm^{-1}) at relatively high concentration and the resolving power of our spectrometer, we estimate that β must be less that 1 cm^{-1}. This is consistent with the values derived from the studies of ^{13}C shifts and intensities, as well as the heavy-doping experiments done by Hochstrasser et al.[20] A better estimate for the bandwidth will be given later from the EPR results.

(B) The Crystal Structure of 1,2,4,5-Tetrachlorobenzene.

The space group[21] for TCB crystals is $P2_1/c$, with two molecules in the unit cell. A phase transition at 188°K changes the lattice into a triclinic space group.[22] The structure of the latter is closely related to the room temperature crystal structure in molecular orientations and unit cell dimensions. The details of the structure for both phases are given in Table II. The stacking of the translationally equivalent molecules is along the a-crystallographic axis in both phases, monoclinic and triclinic. Figure 3 demonstrates the nature of this stacking. From this figure it is clear that the out-of-plane molecular axis is almost

parallel to the axis a. This fact, together with the small length of a compared to b and c lattice constants, leads to the conclusion that this system could be essentially a one-dimensional system,[23,20] implying that the exchange interaction for the triplet state is largest along the a-axis. This is based on a simple view of the nature of $\pi\pi^*$ transitions. In other words, if the molecule is excited into a $\pi\pi^*$ state, the overlap between the different p-orbitals on the two neighboring molecules and the relative orientation[24] in the lattice could be the crucial factors in determining the anisotropy and the sign of energy exchange.

(C) The Optical Detection of Magnetic Resonance in the Lowest Triplet States of TCB Isotopically Mixed Crystals.

Because of the structural similarities between a guest molecule and its perdeutero isotope, isotopically mixed crystals could be formed with any proportions from the guest and host concentrations. Thus the ODMR spectra of highly concentrated crystals (say $\geq 5\%$ H_2) could give not only the spectra of isolated H_2 molecules, but also those of cluster states. Thus a concentration dependence study must be performed in order to isolate the EPR spectra of excited dimers from those of the monomers.

(i) The ODMR Spectra of Monomers.

The ODMR spectra of H_2 and HD traps were observed while monitoring the emission of each trap. Although the ODMR spectrum of HD was easily seen, it was much weaker than the EPR intensity of the deep trap, perhaps because of the loss of spin polarization in the shallow traps due to excitation transfer. The D - |E| spectra consisted of a center peak flanked by three pairs of satellites separated from the main central peak by 7.0, 27.9, and 34.9 MHz. These satellites result from the

coupling between the nuclear hyperfine and nuclear quadrupole moments of the chlorine nuclei to the excited triplet electrons.[16]

The chlorine nuclear quadrupole coupling constants observed for the deep trap were essentially the same as those reported[25] for TCB in durene host; however, the zero field splittings differed. Table III contains the zero field spin Hamiltonian parameters for H_2 in the perdeutero host, and Figure 4 shows a typical ODMR spectrum of H_2 obtained by amplitude modulation of the microwaves. The EPR line at 3560.3 MHz is the shallow trap D - |E| transition detected on the deep trap phosphorescence. At low power (-30 dB), the allowed electron spin transition is quite sharp (< 2.3 MHz) and becomes somewhat broader at higher power (62 mw) with the appearance of the quadrupole satellites. Figure 5 shows the ODMR spectra of the 0.06% H_2 crystal in the region of the allowed spin transition at two different power levels.

(ii) The ODMR Spectra of Dimers.

The high power ODMR spectra of highly concentrated crystals ($\geq 5\%$ H_2) showed the same features of Figure 4 except the allowed electron spin transition became much broader. However, at low powers the transition resolved into a central line which was coincident with electron spin transition of the 0.06% crystal and new satellites which appeared even at -30 dB power level. In Figure 6 the spectrum of the D - |E| transition is shown at two different concentrations and identical output powers. Although the transition at lower frequency was not resolved, it appeared very clearly at higher guest concentration, as shown in Figure 7. The satellites on the D + |E| transition were more resolved (cf. Fig. 8) because of the larger splittings, and became very clear at higher H_2

concentration, as shown in Figure 9.

A complete power dependence study was done on the D - |E| transition. The results clearly indicated that the saturation behavior for the satellites was different from that of the central resonance line. These results are shown in Figure 10, and the spin Hamiltonian parameters for these satellites are given in Table III.

The conclusions of the above experiments are:

(a) The EPR transitions flanking the allowed electron spin transition of the monomer are absent from the zero field ODMR spectra of low concentrated crystals.

(b) The splitting between the two dimer states on the D - |E| transition is 5.7 ± 1 MHz.

(c) The splitting between the two dimer states on the D + |E| transition is 7.6 ± 1 MHz.

(d) The linewidth of the almost resolvable dimer line can be estimated. For the D - |E| transition this is approximately 2 MHz at the appropriate power level.

IV. DISCUSSION

The ordering of the three spin levels of the lowest triplet state of TCB connot be determined from our experiment. However, this ordering is known for TCB in durene.[25] Thus, if there are no severe crystal field perturbations, the ordering in the D_2 host will be the same as in durene. In what follows, we shall use Mulliken's[26] notation for D_{2h} symmetry. Specifically, the z-axis is defined along the C-H bonds, the x-axis as the

out-of-plane of the molecule and the y-axis as in-plane along the halogen bisector. The transformation properties of the spin, orbit and spin-orbital states of a B_{1u} triplet state are shown in Figure 11.

(A) Monomer Spin Hamiltonian

The EPR spectra of the monomer, observed in the low-concentrated crystal (0.06% H_2), can be interpreted by adopting the following spin Hamiltonian

$$H_s(M) = |T_i > D_{ii} < T_i| + \sum_{\alpha=1}^{4} H_Q(\alpha) + \sum_{\alpha=1}^{4} H_{HF}(\alpha) + \sum_{\beta=1}^{2} H_{HF}(\beta) \qquad i = x,y,z \qquad (1)$$

where $|T_i > < T_i|$ is the well-known projection operator, and H_Q and H_{HF} are, respectively, the quadrupole and hyperfine spin Hamiltonians for the αth chlorine nucleus, and β indexes the two protons. The zero field splitting Hamiltonian is written in the principal axes system assuming the molecular symmetry, D_{2h}, is effectively the symmetry of the molecule in the crystal site. D_{ii} are the fine structure tensor elements. It has been shown[16] that the above Hamiltonian can be simplified by utilizing the nature of hyperfine interactions[27] in aromatics. Furthermore, because the ZFS and quadrupole Hamiltonians depend upon S^2 and I^2 respectively, the nuclear quadrupole splittings appear as satellites split from the major zero field electron spin transition by the nuclear quadrupole frequency. Therefore the frequency of the satellites (34.9 MHz and 27.9 MHz) shown in Figure 4 gives the quadrupole coupling constants for ^{35}Cl and ^{37}Cl of the triplet excited state of TCB in the perdeutero host.

The D value refers to the x-axis (cf Fig. 11). The details of these calculations are given in reference (16), and clearly show that in addition to the features mentioned above,a shift in the frequency of the allowed electron spin transition, whose frequency is determined by D_{ii} of Equation 1, is expected if the hyperfine interactions are large or the difference in the energy of $|T_y>$ and $|T_z>$ spin substates is small.[19b] Hence the influence of hyperfine interactions on the dimer spectra is expected to be less than on the monomer spectra if the excitation transfer averages the hyperfine field.[19b,28]

(B) Electron Spin Transitions in the Symmetric and Antisymmetric Dimer States of 1,2,4,5-Tetrachlorobenzene Crystal.

Following Equation 20 of our previous paper,[15] a general spin Hamiltonian for the dimer is

$$H_s(D) = C_A^* C_A H_s(A) + C_B^* C_B H_s(B) \qquad (2)$$

where C is determined by the resonance conditions between the two molecules of the dimer. For translationally equivalent dimers of centrosymmetric molecules, the above Hamiltonian becomes

$$H_s(D) = H_s(A) \equiv H_s(M) \qquad (3)$$

This implies that one EPR transition is expected at the Larmor frequency of the monomer. In other words, although the dimer states, $\psi(+)$ and $\psi(-)$, are separated by 2β, the resonance frequencies are identical in both states.

An exact Hamiltonian for the dimer, with the inclusion of the spin-orbital Hamiltonian, in a properly antisymmetrized basis set results in differences in Larmor frequencies of the $\psi(+)$ and $\psi(-)$

states, as shown in the previous paper.[15] This is because of (a) the selectivity of the spin-orbital operator in coupling the dimer states of the singlet (or higher triplet, for that matter) manifold to the dimer states of the lowest triplet manifold and (b) the difference in the splitting of singlet dimers as compared to triplet dimers. These are related to the more general case of the coupling of the different k states of the lowest triplet band to k states of higher energy singlet or triplet band.[15] The direct relationship between the spread in Larmor frequencies in the band vs. the spread in the states of N-mers is given in Figure 5 of the previous paper[15] and demonstrated in Figure 12 of this paper for a dimer which belongs to a one-dimensional band having the following dispersion.

$$E(k) = E_0 + 2\beta_t \cos ka \tag{4}$$

The exchange interaction is dominant along the a-axis, as in the case of TCB crystal. The position of the monomer and dimer in the k space of the band is also shown in Figure 12. E_0 is the energy of the molecule in the site.

Utilizing the theory given in the previous paper,[15] the microwave dispersion for the dimer is

$$\hbar[\omega_{xz}(\pm) - \omega_{xz}] = \pm\beta_t f_{xz}^{(r)} \tag{5}$$

and

$$\hbar[\omega_{yz}(\pm) - \omega_{yz}] = \pm\beta_t f_{yz}^{(r)} \tag{6}$$

where the reduction factor, f, is given by

$$f_{ij}^{(r)} = |\langle H_{SO}^{(r)} \rangle_{ij}|^2 \, (\beta_s/\beta_t - 1)\Delta E_{st}^{-2} \qquad (7)$$

for a microwave transition between the levels $|T_i\rangle$ and $|T_j\rangle$ and r is the specific spin-orbit axis. A simple fact emerges from this theory; namely, that the optical splitting, $2\beta_t$, of the dimer (1-10 cm^{-1} in triplet states) is reduced by f_{ij} into the magnetic region (megahertz) due to the anisotropy in the spin-orbital interactions. Hence the dynamics of coherence could be studied in a more rigorous way since the correlation time for the experiments now approaches the coherent limit. Comparing Equations 5 and 6 to those of the exciton[15] at k = 0 and k = π/a of the first Brillouin zone, we get

$$[\Delta\omega_{xz}(k=0) - \Delta\omega_{xz}(k=\pm\pi/a)] = 2[\Delta\omega_{xz}(K=1) - \Delta\omega_{xz}(K=2)] \qquad (8)$$

and

$$[\Delta\omega_{yz}(k=0) - \Delta\omega_{yz}(k=\pm\pi/a)] = 2[\Delta\omega_{yz}(K=1) - \Delta\omega_{yz}(K=2)] \qquad (9)$$

where K labels the states of the dimer.

Our experiments demonstrate the validity of the above equations for one-dimensional systems. Figure 13 and 14 contain the experimental results on the dimers of 1,2,4,5-tetrachlorobenzene crystal, represented by the dashed vertical bars, and the so-called double-hump curves of the exciton for both the D + |E| and D - |E| transitions[23] (xz and yz transitions). These findings are in excellent agreement with those calculated based on the theory developed in the previous paper.[15] Moreover, these observations indicate that the zero field EPR transitions

in the two dimer states are different and that from the dimer spectrum one can extrapolate to predict the resonances of the different k states and hence a map for the density of states can be drawn for the triplet exciton. It should be noted that these magnetic resonance experiments resemble those of optical heavy-doping[29,19a] and resonance multiplet[30,19b] experiments in the sense that the rf field samples the triplet states of randomly distributed aggregates, hence the spectrum of different clusters could be recorded, but the time scale of the microwave experiments clearly allowed us to investigate the phase losses in the dimer states more quantitatively, as will be demonstrated in the coming sections.

(C) Electron Spin Coherence in the Symmetric and Antisymmetric Dimer States.

An accurate treatment for the intensities of the microwave transitions in the plus and minus states requires a quantitative evaluation of the population distribution in the spin sublevels of the two states, including spin-lattice relaxation, spin-spin relaxation and the scattering mechanism. At low temperatures the spin-lattice relaxation could be neglected in phosphorescent triplet states.[31] The establishment of Boltzmann statistics depends to a large extent on the dynamics of scattering. In this regime, the partition function for a three-level [$\psi(+)$, $\psi(-)$ and $\psi(M)$] system is given by

$$z = g_- + g_+ \exp(-2\beta/kT) + g_M \exp(-\beta/kT) \qquad (10)$$

where the energy of $\psi(-)$ is taken to be zero and g is the number of states. Thus at a fixed temperature the intensity ratio of the plus

and minus states is directly related to the resonance interaction, β_t.

As shown in the previous paper,[15] the scattering of triplet excitation by phonons can be understood from the magnetic resonance spectra if we incorporate the scattering probabilities into Bloch magnetic equations[32] for the spin ensemble which has a net "pseudo" magnetization in the interaction representation. In the rotating frame these equations are given in terms of the scattering probabilities (τ_{+-}^{-1}, τ_{-+}^{-1}) and the fraction of spin in each of the two states of the dimer:[15]

$$[dG_+/dt] = i[N_+\omega_1 M_0 - \Delta\hat{\omega}_+ G_+] + (G_-/\tau_{-+}) - (G_+/\tau_{+-}) \qquad (11)$$

and

$$[dG_-/dt] = i[N_-\omega_1 M_0 - \Delta\hat{\omega}_- G_-] + (G_+/\tau_{+-}) - (G_-/\tau_{-+}) \qquad (12)$$

where ω_1 is simply γH_1, and the components of the complex moment G determine the microwave absorption in the dimer:

$$\begin{aligned} u &= u_+ + u_- \\ v &= v_+ + v_- \\ M_z &= M_{z+} + M_{z-} \end{aligned} \qquad (13)$$

The solution of these equations in the steady state for the different limits, slow, intermediate and fast exchange (cf Figure 7 through 10 of the previous paper[15]) shows the sensitivity of the microwave lineshape to the cross-section for the scattering of the excitons by phonons.

With the above considerations in mind, a coherence time on the order of 10^{-7} sec was obtained from the optically detected magnetic

resonance spectra of the dimer. For accurate determination of the coherence time, well-resolved spectra are needed. However, it is clear from Figures 7 and 8 and Equation 78 of the previous paper[15] that for a good resolution between the two transitions of the dimer, the coherence time must lie between 10^{-6} and 5×10^{-7} sec. Another way for obtaining the coherence time is from the measurements of the linewidth of the EPR transitions if the linewidth is completely determined by the scattering time. The crystal field inhomogeneity and hyperfine effects make the apparent width measure a lower limit on the coherence time. Therefore the approximately 2 MHz linewidth of the $\psi(+)$ state of tetrachlorobenzene dimers gives a coherence time of 5×10^{-7} sec or longer.

The excellent agreement between the predictions of the theory in the previous paper[15] and the results of this paper indicate that the dimer is due to translationally equivalent molecules and that the triplet exciton band in tetrachlorobenzene crystal is one-dimensional, confirming the findings of Francis and Harris[23] on the <u>neat</u> crystal studies. To calculate the resonance interaction between the two molecules, one needs an accurate measurement of the intensity ratio of the EPR transitions, which is not at hand in this case because of the spectral overlap. However, the dimer EPR spectra show that the peak intensities are different, in agreement with the calculated (cf Figure 6 of the previous paper[15]) and the observed[23] resonance spectra for the excitons. This implies that the two states are not equally populated if the linewidths of the $\omega(+)$ and $\omega(-)$ transitions are the same. Otherwise the intensity distribution in both $\psi(+)$ and $\psi(-)$ states will be identical (cf Figure 7 of reference 15). In a Boltzmann regime the estimated ratio

(1.3) for the intensities of $\omega(+)$ and $\omega(-)$ gives a resonance interaction matrix element, $\beta = 0.15\ cm^{-1}$ and hence an exciton bandwidth of $0.6\ cm^{-1}$ (cf Figures 8-10 of the previous paper[15]). The important point to remember is that the transfer time in this system must be less than 10^{-10} sec., with a maximum value of 16×10^{-12} sec, and therefore the coherence time of the state exceeds the stochastic limit by orders of magnitude. Quantitative measurements of these coherence times and their connection to the nature of scattering channels are under study. We expect that the different models, linear, quadratic, etc., for exciton-phonon scattering will result in sufficiently different scattering probabilities, which are incorporated into the line shape function, that they can ultimately be distinguished experimentally for the dimer and hopefully an extrapolation to the exciton dynamics can be drawn.

V. ACKNOWLEDGEMENT

This work was supported in part by the National Science Foundation and in part by the Inorganic Materials Research Division of Lawrence Berkeley Laboratory under the auspices of the U.S. Atomic Energy Commission.

REFERENCES

1. A. S. Davydov, Theory of Molecular Excitons, McGraw-Hill Pub. Co., New York, NY (1962).

2. J. Jortner, S. A. Rice, J. L. Katz and S. I. Choi, J. Chem. Phys. 42, 309 (1965).

3. V. Ern, A. Suna, T. Tomkiewicz, P. Avakian and R. P. Groff, Phys. Rev. B 5, 3222 (1972).

4. A. H. Francis and C. B. Harris, J. Chem. Phys. 55, 3595 (1971).

5. A. H. Francis and C. B. Harris, Chem. Phys. Lett. 9, 181 (1971).

6. M. A. El-Sayed, M. T. Wauk and G. W. Robinson, Mol. Phys. 5, 205 (1962); G. C. Nieman and G. W. Robinson, J. Chem. Phys. 37, 2150 (1962); H. Sternlicht, G. C. Nieman and. G. W. Robinson, J. Chem. Phys. 38, 1326 (1963).

7. R. E. Merrifield, J. Chem. Phys. 28, 647 (1958).

8. R. E. Merrifield, J. Chem. Phys. 48, 4318 (1968); R. C. Johnson, R. E. Merrifield, P. Avakian and R. B. Flippen, Phys. Rev. Lett. 19, 285 (1967); R. P. Groff, R. E. Merrifield and P. Avakian, Chem. Phys, Lett. 5, 168 (1970).

9. A. S. Davydov, Theory of Molecular Excitons, Plenum Press, New York (1971) and references therein; A. B. Zahlan, in Excitons, Magnons and Phonons, ed. A. B. Zahlan, Cambridge University Press (1968); ibid., M. A. El-Sayed and W. R. Moomaw, p. 103; R. M. Hochstrasser and P. N. Prasad, J. Chem. Phys. 56, 2814 (1972); R. Kopelman, F. W. Ochs and P. N. Prasad, J. Chem. Phys. 57, 5409 (1972); V. L. Broude and V. K. Dolganov, Sov. Phys. Solid State 14, 225 (1972); V. K. Dolganov and E. F. Sheka, Sov. Phys. Solid State 15, 576, 595 (1973); F. B. Slobodskoi and E. F. Sheka, ibid. 15, 860 (1973); G. J. Small, J. Chem. Phys. 58, 2015 (1973).

10. H. Sternlicht and H. McConnell, J. Chem. Phys. 35, 1793 (1961); Z. G. Soos, J. Chem. Phys. 51, 2107 (1969); V. D. Haarer and H. C. Wolf, Mol. Cryst. 10, 359 (1970); M. Sharnoff and E. B. Iturbe, Phys. Rev. Lett. 27, 576 (1971); D. M. Hanson, Chem. Phys. Lett. 11, 175 (1971).

11. T. Holstein, Ann. Phys. (N.Y.) 8, 325 (1959); T. Holstein, Ann. Phys. (N.Y.) 8, 343 (1959).

12. M. Grover and R. Silbey, J. Chem. Phys. 54, 4843 (1971).

13. R. W. Munn and W. Siebrand, J. Chem. Phys. 52, 47 (1970).

REFERENCES (continued)

14. C. B. Harris and M. D. Fayer, Phys. Rev. B XX, XXX (1974).

15. A. H. Zewail and C. B. Harris, Phys. Rev. B XX, XXX (1974).

16. M. J. Buckley and C. B. Harris, J. Chem. Phys. 56, 137 (1971).

17. The perdeutero materials used in these experiments were taken from the same batch used in the experiments of reference 18.

18. M. Fayer and C. B. Harris, Phys. Rev. B 9, 748 (1974).

19. (a) R. M. Hochstrasser and J. D. Whiteman, J. Chem. Phys. 56, 5945 (1972).
(b) R. M. Hochstrasser and A. H. Zewail, Chem. Phys. 4, 142 (1974).

20. R. M. Hochstrasser, T. Li, H.-N. Sung, J. E. Wessel and A. H. Zewail, Pure and Appl. Chem. 37, 85 (1974).

21. C. Dean, M. Pollak, B. M. Craven and G. A. Jeffrey, Acta Cryst. 11, 710 (1958).

22. A. Monfils, Compt. Rend. 241, 561 (1955); G. Gafner and F. H. Herbstein, Acta Cryst. 13, 702, 706 (1960); F. H. Herbstein, Acta Cryst. 18, 997 (1965).

23. A. H. Francis and C. B. Harris, Chem. Phys. Lett. 9, 188 (1971).

24. J. M. Schurr, Mol. Phys. 27, 357 (1974).

25. A. H. Francis and C. B. Harris, J. Chem. Phys. 57, 1050 (1972).

26. R. S. Mulliken, J. Chem. Phys. 23, 1997 (1955).

27. J. S. Vincent and A. H. Maki, J. Chem. Phys. 42, 865 (1965); Y. Gondo and A. H. Maki, J. Chem. Phys. 50, 3270 (1969); see also references 16, 19b and references therein.

28. C. A. Hutchison, Jr., and J. S. King, Jr., J. Chem. Phys. 58, 892 (1973).

29. H.-K. Hong and G. W. Robinson, J. Chem. Phys. 52, 825 (1970); ibid. 54, 1369 (1971).

30. D. Hanson, J. Chem. Phys. 52, 3409 (1970).

31. J. H. van der Waals and M. S. de Groot, in The Triplet State, ed. A. B. Zahlan, Cambridge University Press, London (1967).

REFERENCES (continued)

32. F. Bloch, Phys. Rev. 70, 460 (1946).

Table I

Composition of the Isotopically Mixed Crystals of 1,2,4,5-Tetrachlorobenzene*

Crystal	Percentage Composition		
	H_2	HD	D_2
A**	0.06	4.63	95.31
B	5.7	5.0	89.3
C	11.8	5.2	83.0

* From the analysis of the Mass Spectra

** The analysis of this sample was done by NMR since the intensity of H_2 in the mass spectrum was not appreciable.

Table II

Crsytallographic Data for the Monoclinic and the Triclinic Phases of 1,2,4,5-Tetrachlorobenzene*

	Triclinic	Monoclinic
Temperature	below 188 ± 2°K	∿ 300°K
phase	α	β
space group	P1 or $P\bar{1}$	$P2_1/c$
c(Å)	9.60	9.73
b(Å)	10.59	10.63
a(Å)	3.76	3.86
α	95°	90°
β	102 1/2	103 1/2
γ	92 1/2	90
Z**	2	2
Molecular Symmetry	C_1	C_i

* See the text for the references

** The number of molecules per unit cell.

Table III

Spin Hamiltonian Parameters For the Lowest Triplet State of 1,2,4,5-Tetrachlorobenzene-h_2 Monomers and Dimers in the Perdeutero Host

(MHz)	Dimer		Monomer
	$\psi(+)$	$\psi(-)$	$\psi(M)$
$D + \|E\|$	5542.0	5534.4	5539.6
$D - \|E\|$	3580.9	3575.2	3577.8
$2\|E\|$	1961.1	1959.2	1961.8

FIGURE CAPTIONS

Figure 1. Experimental arrangement for the optical detection of magnetic resonance in zero applied magnetic field.

Figure 2. Phosphorescence spectra of isotopically mixed 1,2,4,5-tetrachlorobenzene crystals at different guest (H_2) concentrations. The percentage composition of these crystals, A to C, is listed in Table I. The B and C spectra were taken at 4.2°K while the A spectrum was recorded at 1.8°K. The strongest band in the spectra is due to H_2 guest emission and the bands at higher energy are due to HD and D_2 emission.

Figure 3. The stacking of 1,2,4,5-tetrachlorobenzene molecules in the crystal lattice along the translational axis, a. It is clear from the figure that the normal to the molecular plane is approximately parallel to the a-crystallographic axis.

Figure 4. Zero field optically detected magnetic resonance ($D - |E|$) spectrum of 1,2,4,5-tetrachlorobenzene-h_2 traps in 1,2,4,5-tetrachlorobenzene-d_2 host at 1.7K. The optical emission of H_2 was isolated from HD and D_2 emission by the monochromator (cf Figure 1).

Figure 5. EPR $D - |E|$ transition of 1,2,4,5-tetrachlorobenzene-h_2 traps in the D_2 host at two different power levels. The frequency given, 3577.8 MHz, is the peak position.

Figure 6. Zero field ODMR spectra (D - |E| transition) of isotopically mixed 1,2,4,5-tetrachlorobenzene crystals for two different guest (H_2) concentrations: (a) is the 5.7% H_2 crystal and (b) is the 0.06% H_2 crystal. The output microwave power was the same for spectra of both (a) and (b).

Figure 7. Zero field ODMR spectrum of 1,2,4,5-tetrachlorobenzene monomers and dimers (D - |E| transition) in the 11.8% H_2 crystal. The figure clearly shows that the Larmor frequency of $\psi(+)$ and $\psi(-)$ dimer states is different from the monomer frequency.

Figure 8. Zero field ODMR spectra (D + |E| transition) of isotopically mixed 1,2,4,5-tetrachlorobenzene crystals for two different guest (H_2) concentrations: (a) is the 5.7% H_2 crystal and (b) is the 0.06% H_2 crystal. The output microwave power was the same for spectra of both (a) and (b).

Figure 9. Zero field ODMR spectrum of 1,2,4,5-tetrachlorobenzene monomers and dimers (D + |E| transition) in the 11.8% H_2 crystal. The figure clearly shows that the Larmor frequency of $\psi(+)$ and $\psi(-)$ dimer states is different from the monomer frequency.

Figure 10. Ratio of dimer to monomer D - |E| transition intensities (I_D/I_M) at different output power levels. The experimental points in the figure were taken from the zero field ODMR spectrum of the same crystal.

Figure 11. The symmetry of triplet state sublevels of 1,2,4,5-tetrachlorobenzene monomer. The group theoretical transformation properties of the spin and spin-orbit states of a $^3B_{1u}$ state is given in the coordinate system described at the top of the figure.

Figure 12. The figure on the left shows the energy for a one-dimensional exciton as a function of k. The solid line at $k = \pi/2a$ represents the location of the monomer in the band in the absence of host polarization and/or hyperfine effect. The dashed lines give the position of $\psi(+)$ and $\psi(-)$ dimer states in the band. The figure on the right gives both the energy and microwave dispersion for the whole band. The correspondence between the energy spread, $E(\pm)$ and $E(M)$, and the spread in Larmor frequencies, $\omega(\pm)$ and $\omega(M)$, for both the dimer and monomer states is represented by the dashed lines.

Figure 13. Dimer and exciton $D - |E|$ transition of 1,2,4,5-tetrachlorobenzene crystal. The dashed vertical bars in the figure represent the experimental frequencies of $\psi(+)$ and $\psi(-)$ dimer states and the width of these bars is the estimated error on these frequencies. The exciton spectrum is the band-to-band microwave transitions taken from reference 23 for the neat H_2 crystal.

Figure 14. Dimer and exciton $D + |E|$ transition of 1,2,4,5-tetrachlorobenzene crystal. The dashed vertical bars represent the experimental freqencies of $\psi(+)$ and $\psi(-)$ dimer states, and the width of these bars is the estimated error on these frequencies. The exciton spectrum is the band-to-band microwave transitions taken from reference 23 for the neat

Figure 14 (continued): H_2 crystal. The dynamics governing the intensity distribution in the ODMR spectra of $\psi(+)$ and $\psi(-)$ states depend on the transition dipole strength and the nature of the decay channel from each state (see the text and reference 15); the experimental intensity distribution is not shown in the figure.

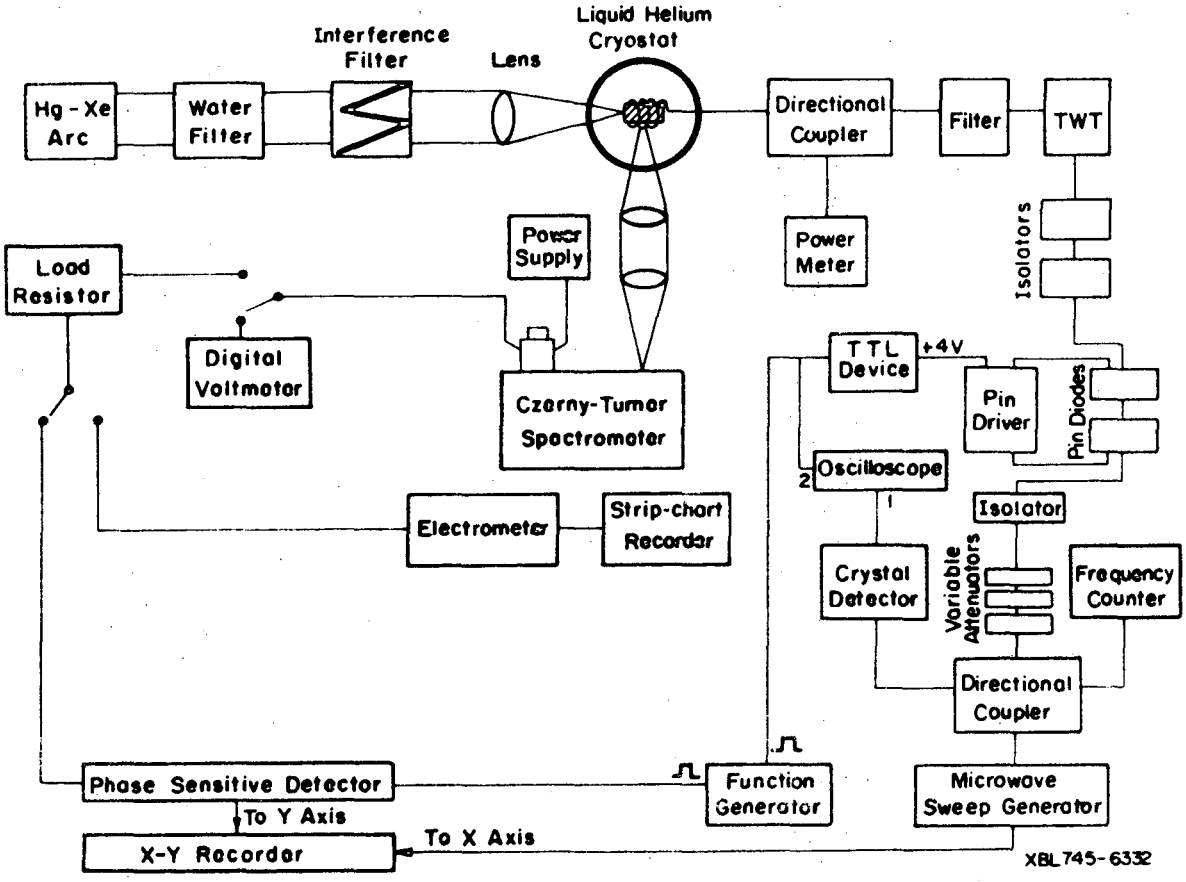
Hg - Xe Arc
Water Filter
Interference Filter
Lens
Liquid Helium Cryostat
Directional Coupler
Filter
TWT
Power Meter
Isolators
Power Supply
Load Resistor
Digital Voltmeter
Czerny-Turner Spectrometer
TTL Device
+4V
Pin Driver
Pin Diodes
Oscilloscope
2
1
Isolator
Electrometer
Strip-chart Recorder
Crystal Detector
Variable Attenuators
Frequency Counter
Directional Coupler
Phase Sensitive Detector
Function Generator
Microwave Sweep Generator
To Y Axis
To X Axis
X-Y Recorder
XBL745-6332

Fig. 1

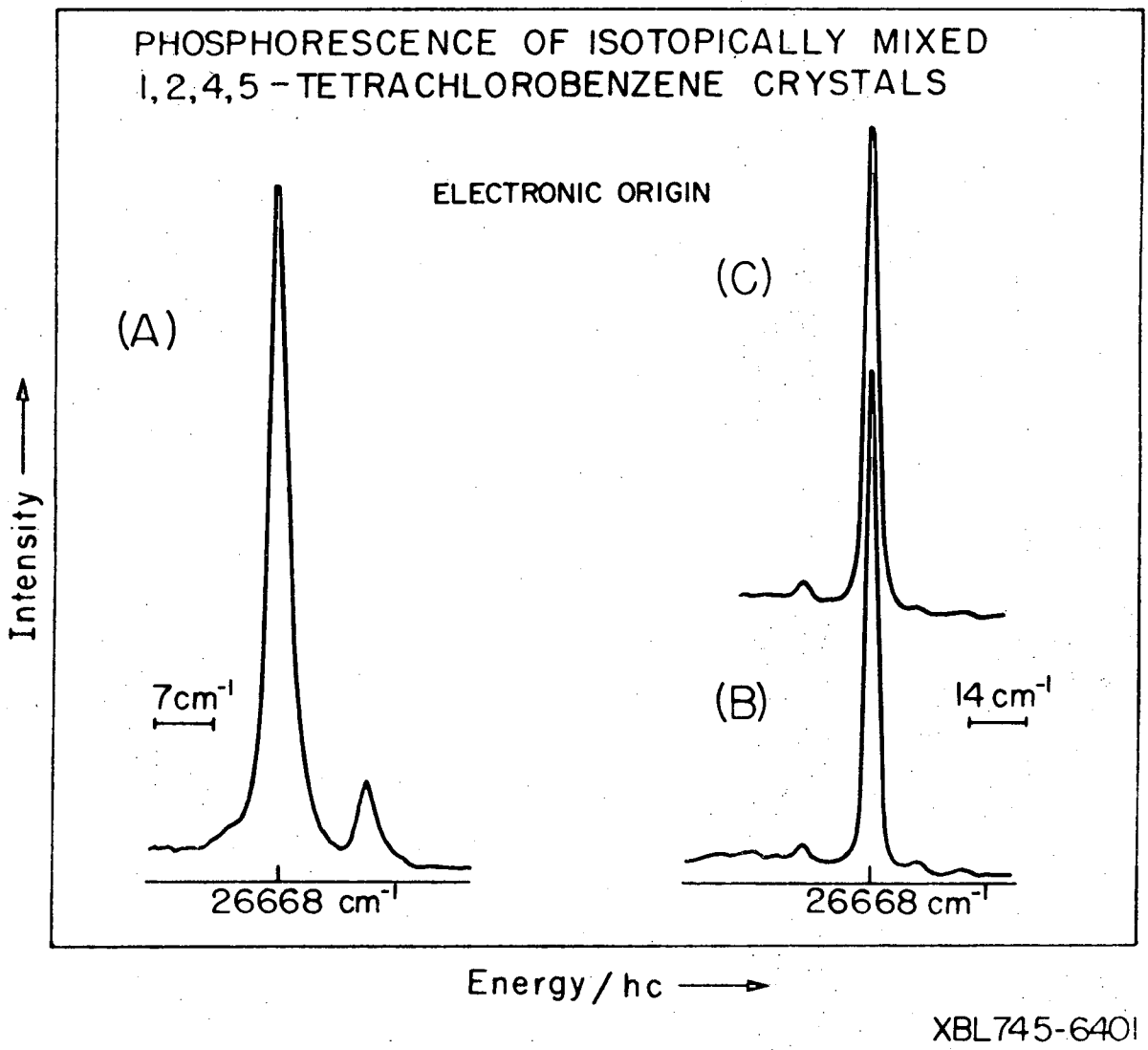
PHOSPHORESCENCE OF ISOTOPICALLY MIXED
1,2,4,5-TETRACHLOROBENZENE CRYSTALS
ELECTRONIC ORIGIN
(A)
(B)
(C)
7cm⁻¹
14 cm⁻¹
26668 cm⁻¹
26668 cm⁻¹
Intensity
Energy / hc
XBL745-6401

Fig. 2

STACKING OF 1,2,4,5-TETRACHLOROBENZENE MOLECULES IN THE CRYSTAL

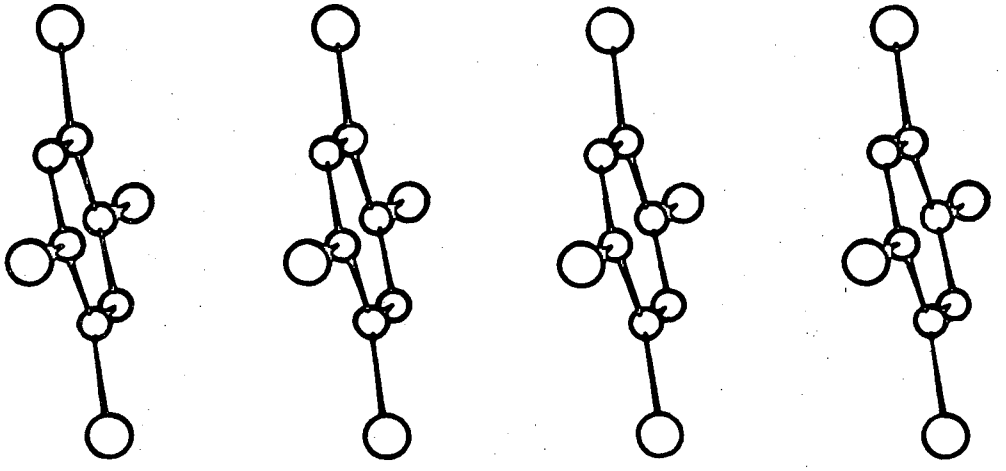

TRANSLATIONAL AXIS ⟶

XBL 745-6333

Fig. 3

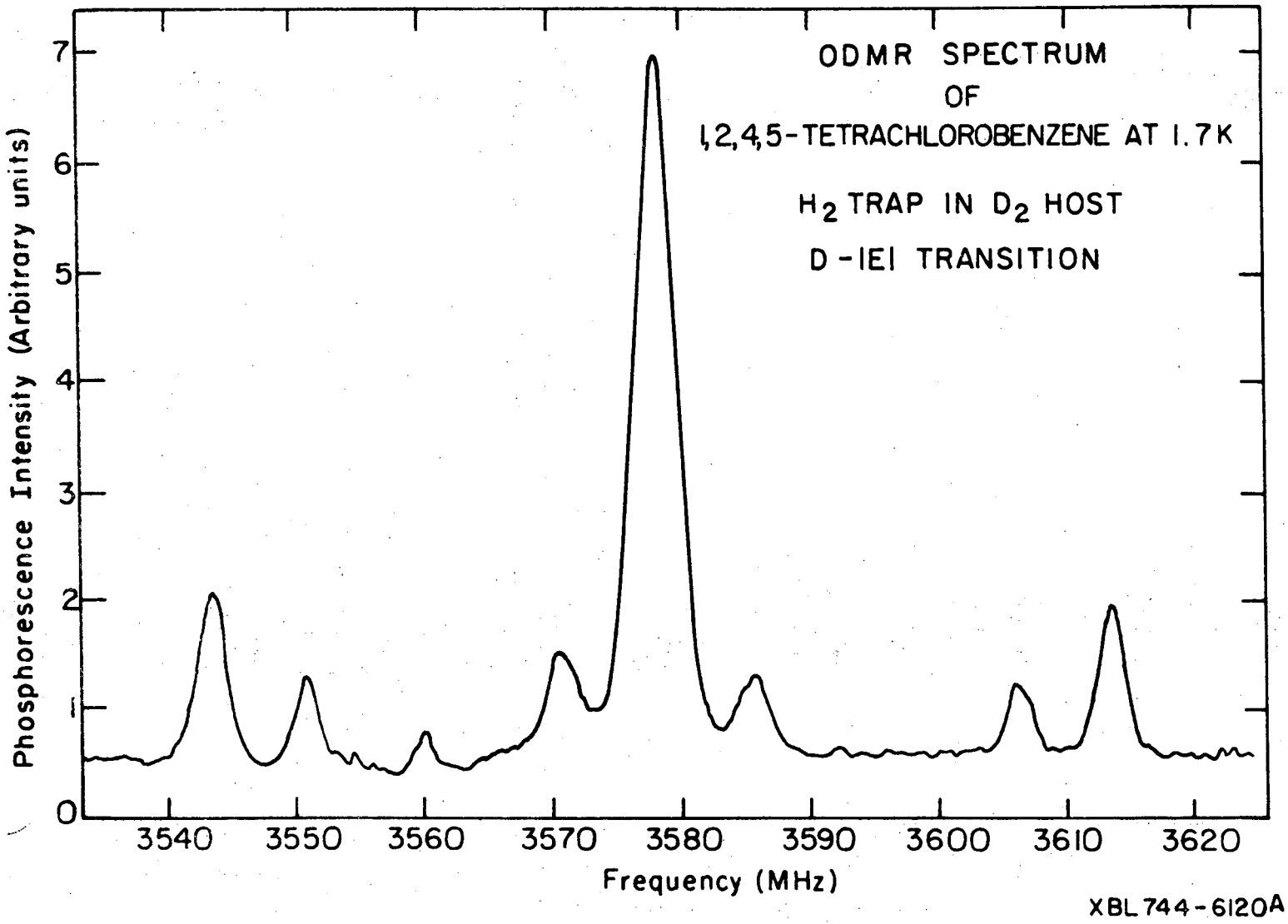
ODMR SPECTRUM
OF
1,2,4,5-TETRACHLOROBENZENE AT 1.7K
H_2 TRAP IN D_2 HOST
D - |E| TRANSITION
Phosphorescence Intensity (Arbitrary units)
0
1
2
3
4
5
6
7
3540
3550
3560
3570
3580
3590
3600
3610
3620
Frequency (MHz)
XBL 744-6120A

Fig. 4

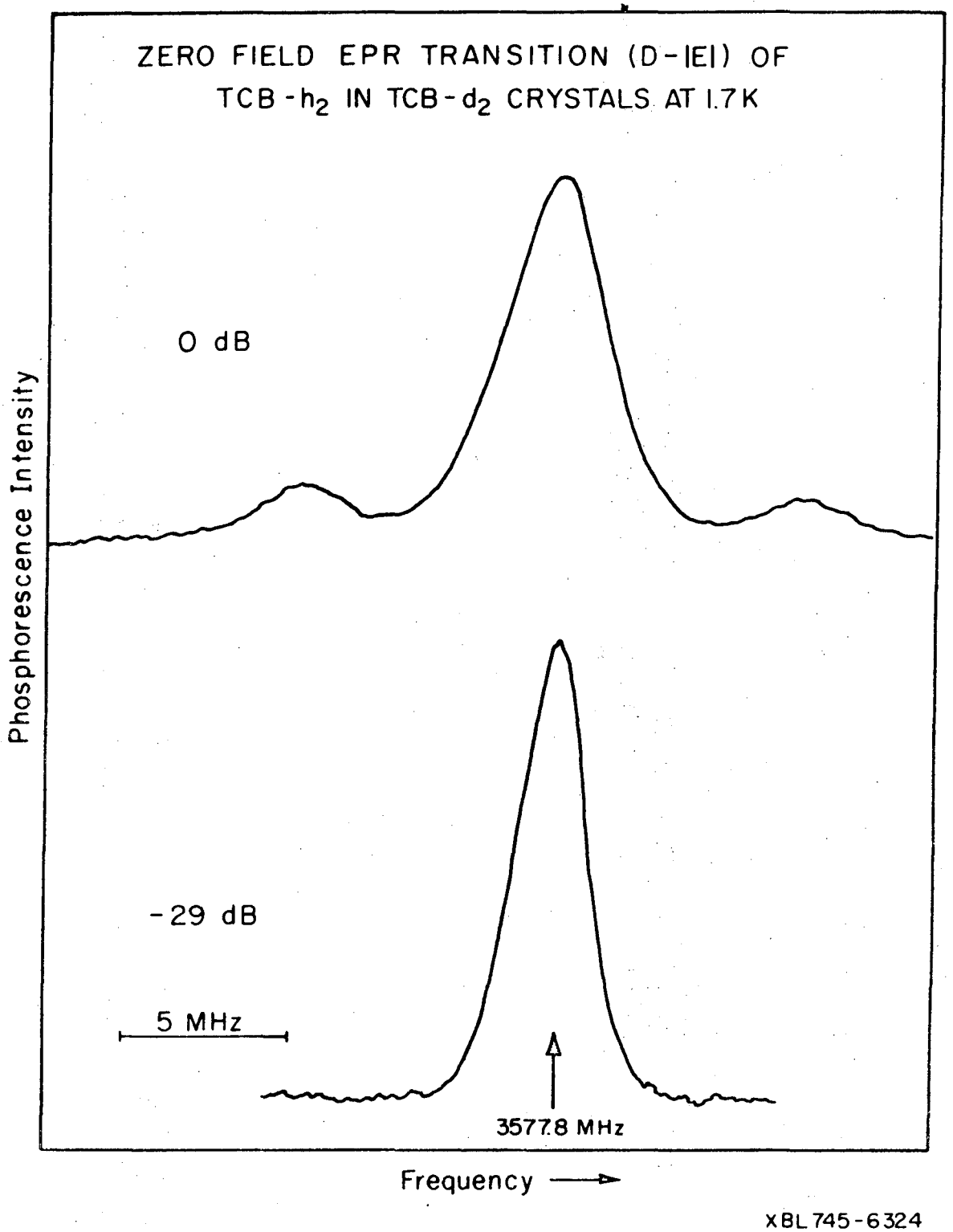
ZERO FIELD EPR TRANSITION (D-|E|) OF
TCB-h_2 IN TCB-d_2 CRYSTALS AT 1.7K
0 dB
-29 dB
5 MHz
3577.8 MHz
Phosphorescence Intensity
Frequency
XBL745-6324

Fig. 5

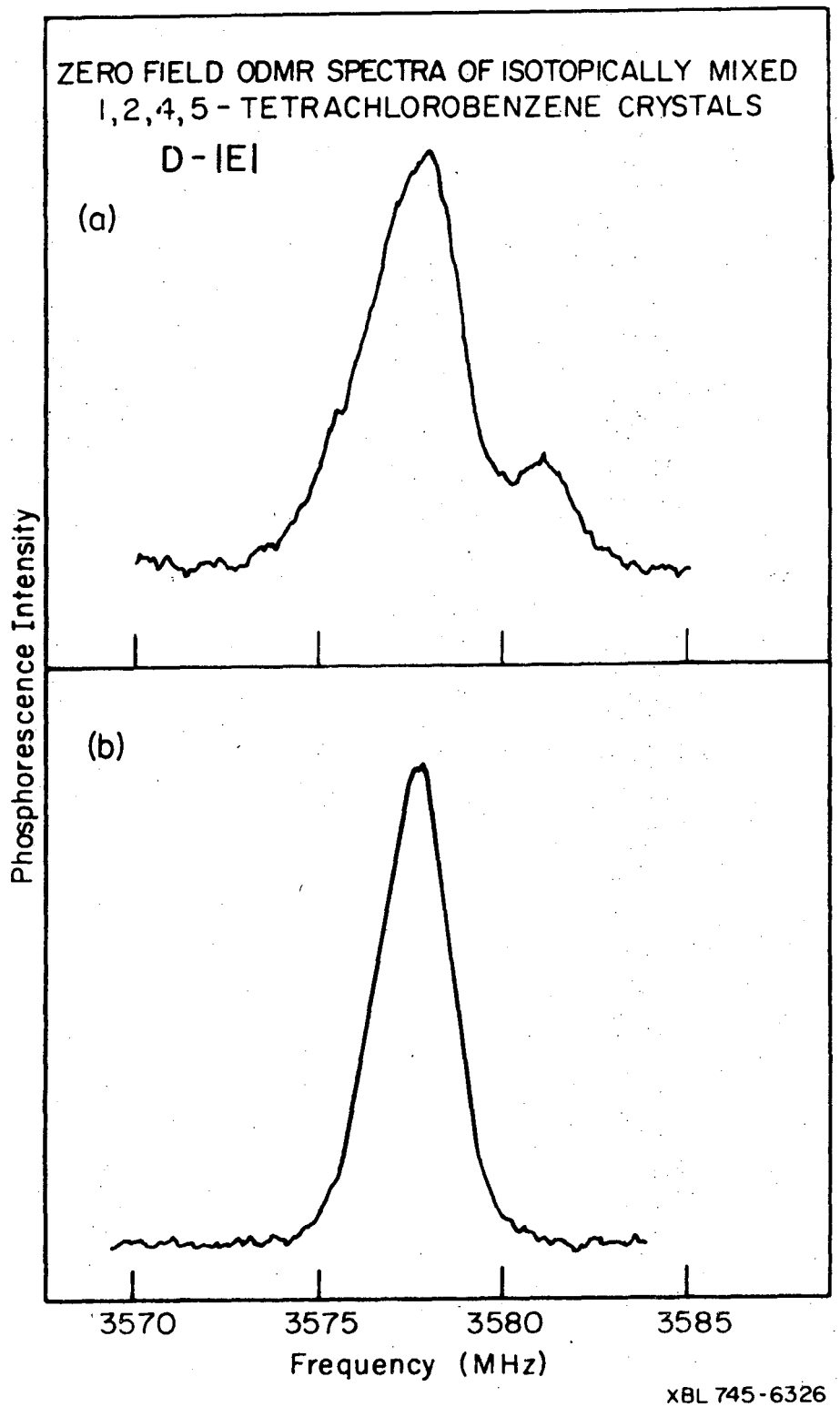
ZERO FIELD ODMR SPECTRA OF ISOTOPICALLY MIXED
1,2,4,5 - TETRACHLOROBENZENE CRYSTALS
D - |E|
(a)
(b)
Phosphorescence Intensity
3570
3575
3580
3585
Frequency (MHz)
XBL 745-6326

Fig. 6

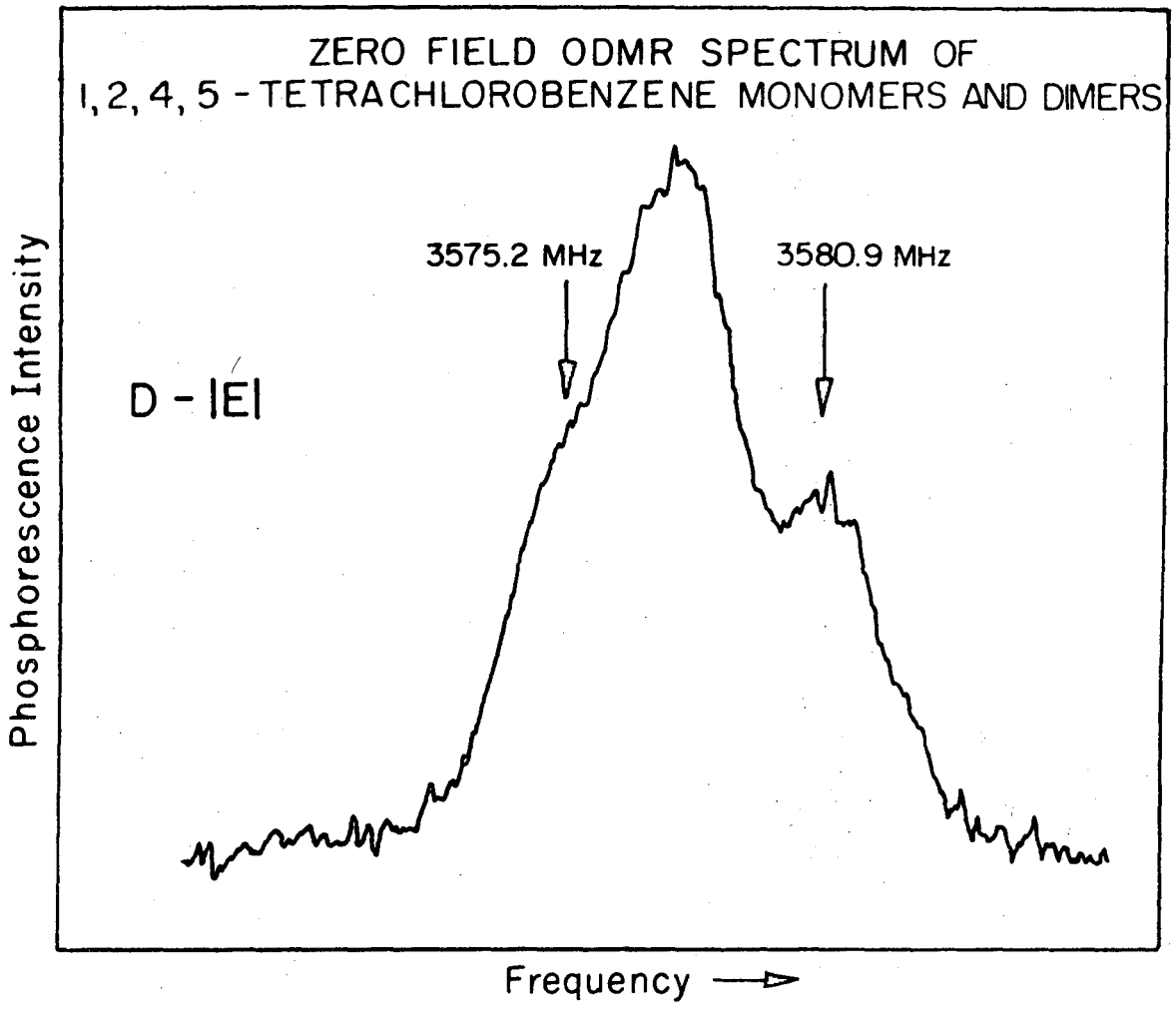
ZERO FIELD ODMR SPECTRUM OF
1,2,4,5 - TETRACHLOROBENZENE MONOMERS AND DIMERS
3575.2 MHz
3580.9 MHz
D - |E|
Phosphorescence Intensity
Frequency
XBL745 - 6329

Fig. 7

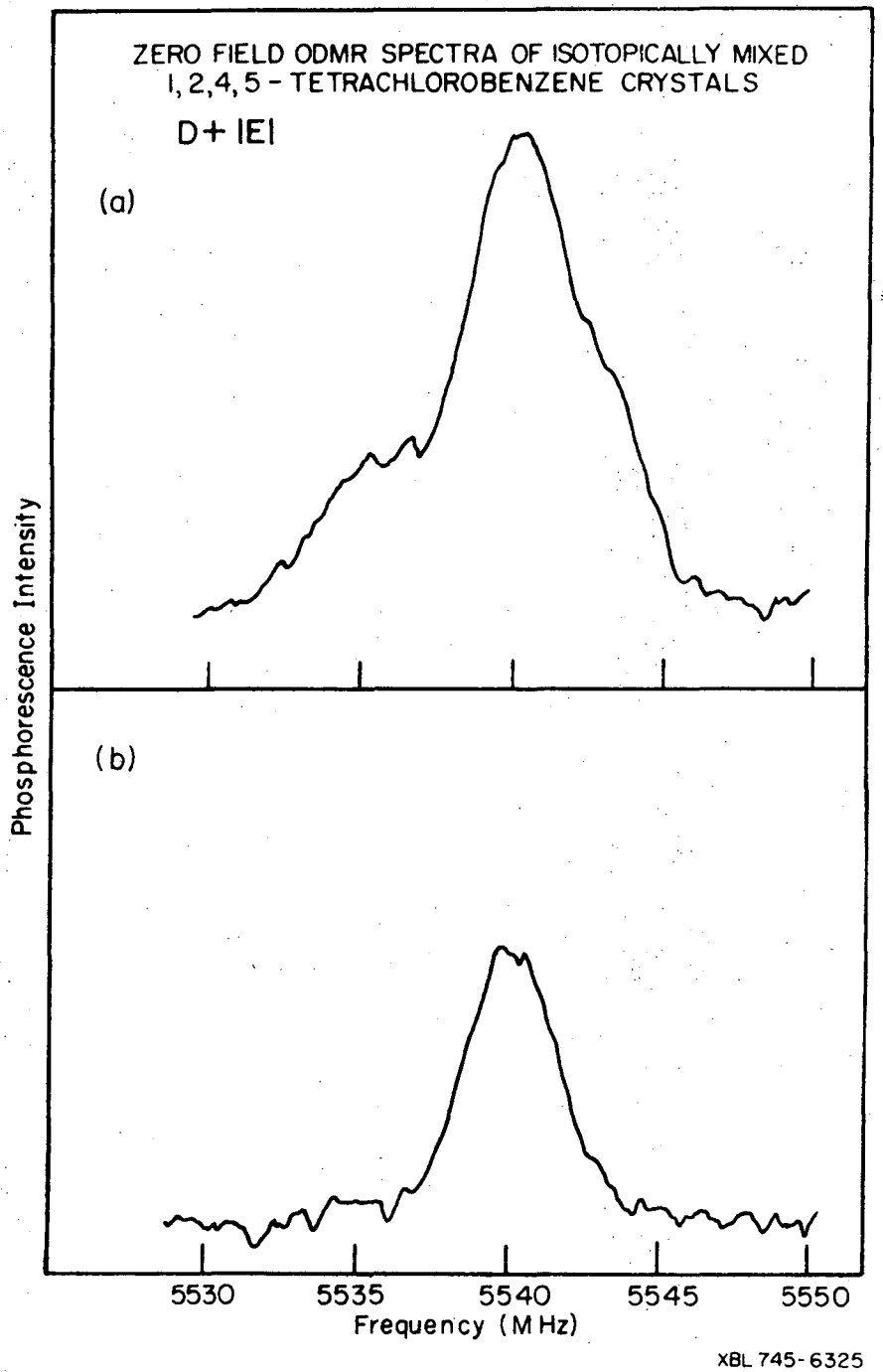
ZERO FIELD ODMR SPECTRA OF ISOTOPICALLY MIXED
1, 2, 4, 5 - TETRACHLOROBENZENE CRYSTALS
D+ |E|
(a)
(b)
Phosphorescence Intensity
5530
5535
5540
5545
5550
Frequency (MHz)
XBL 745-6325

Fig. 8

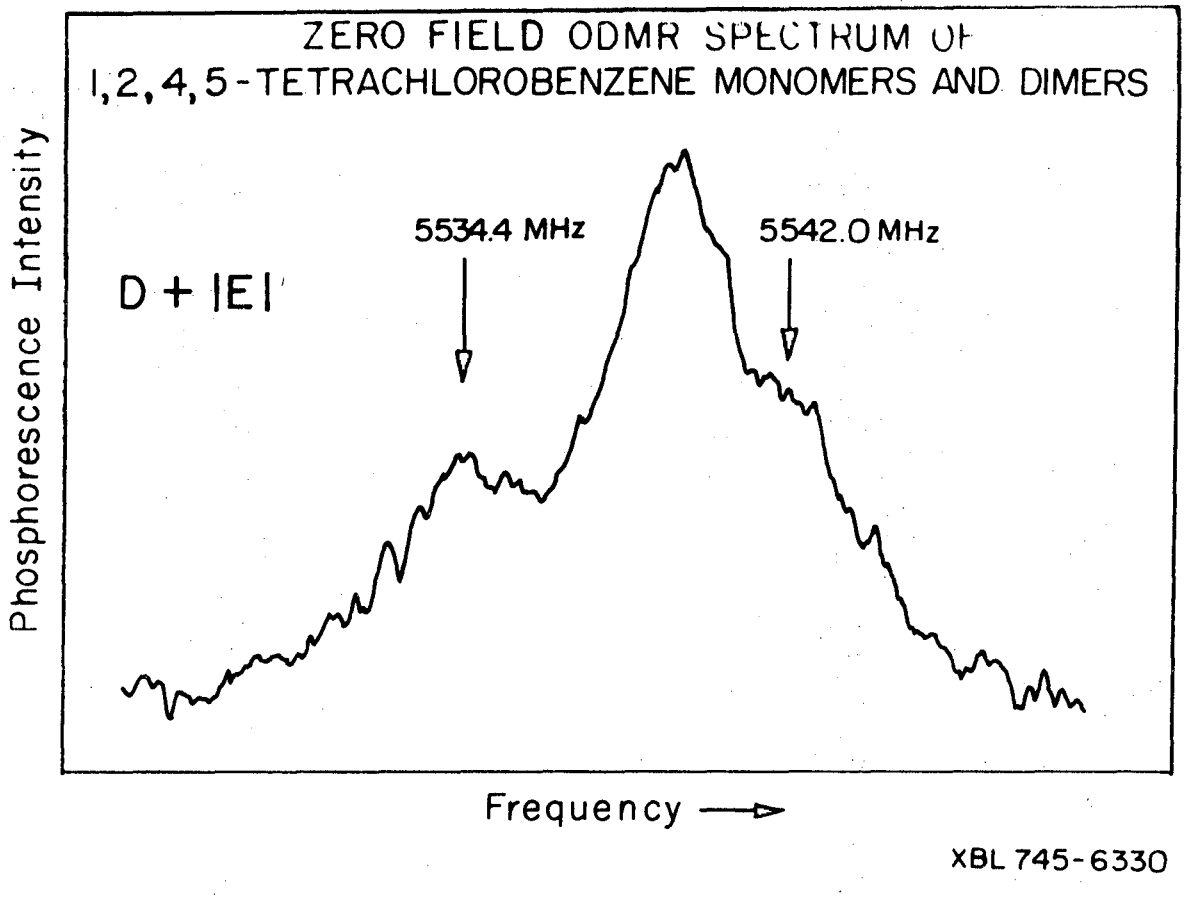
ZERO FIELD ODMR SPECTRUM OF
1,2,4,5-TETRACHLOROBENZENE MONOMERS AND DIMERS
5534.4 MHz
5542.0 MHz
D + |E|
Phosphorescence Intensity
Frequency
XBL 745-6330

Fig. 9

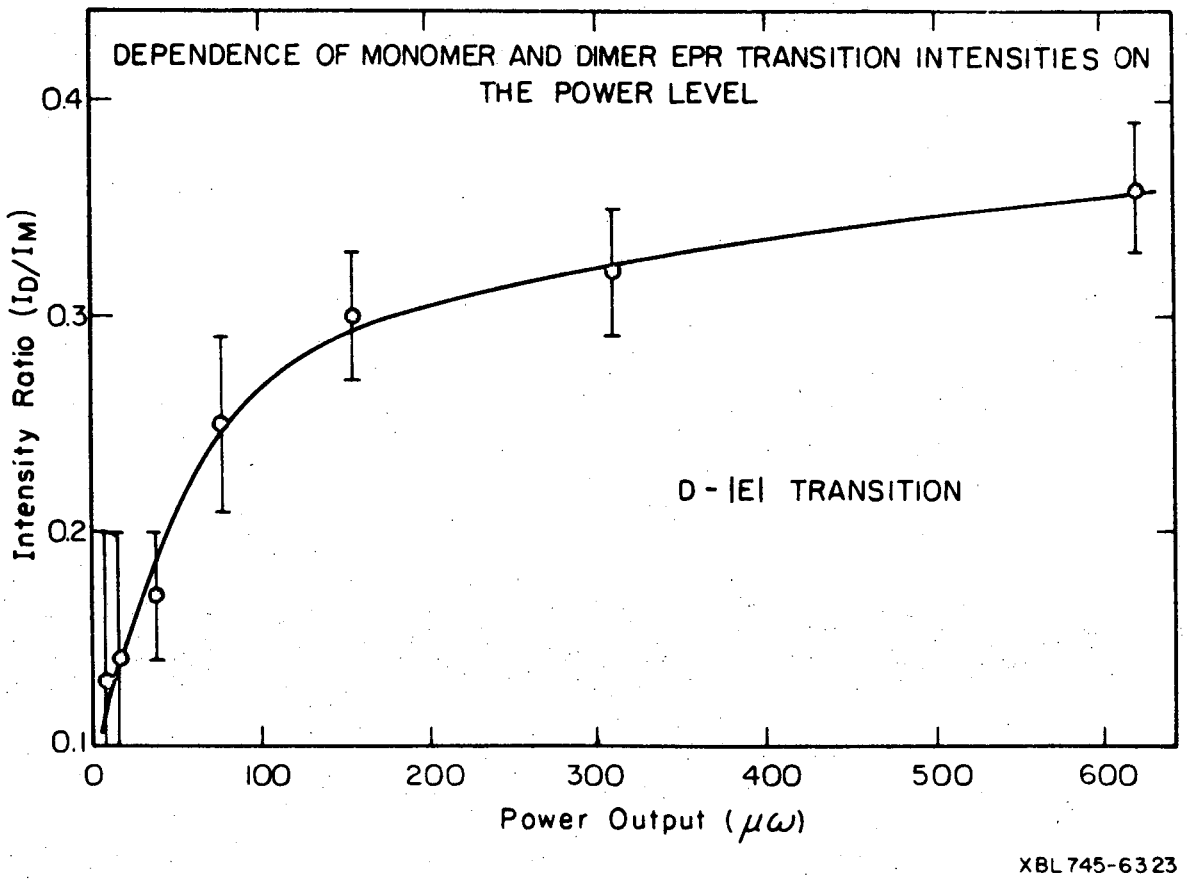
DEPENDENCE OF MONOMER AND DIMER EPR TRANSITION INTENSITIES ON THE POWER LEVEL
Intensity Ratio (I_D/I_M)
0.4
0.3
0.2
0.1
D - |E| TRANSITION
0
100
200
300
400
500
600
Power Output ($\mu\omega$)
XBL745-6323

Fig. 10

SYMMETRY OF TRIPLET STATE SUBLEVELS IN TETRACHLOROBENZENE MONOMER

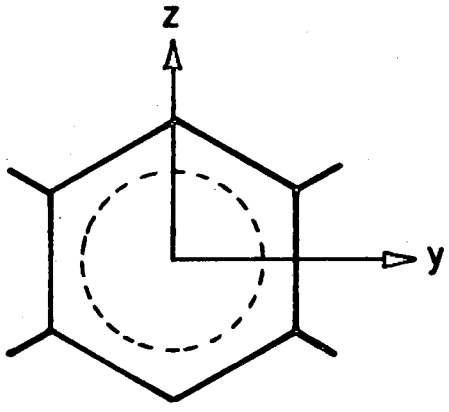

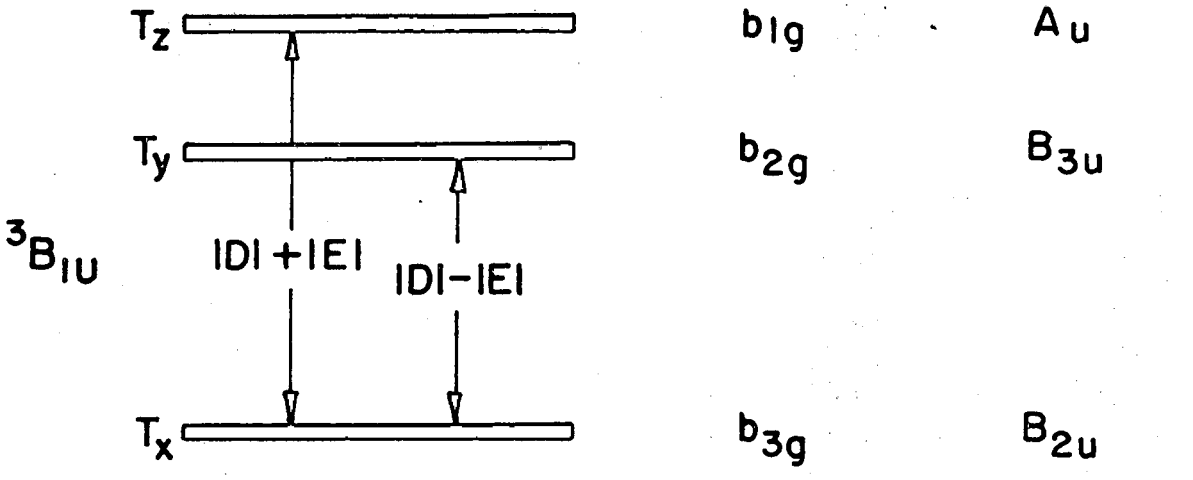

XBL745-6321

Fig. 11

THE RELATIONSHIP BETWEEN EXCITON AND DIMER DISPERSIONS
IN ONE-DIMENSIONAL CRYSTAL

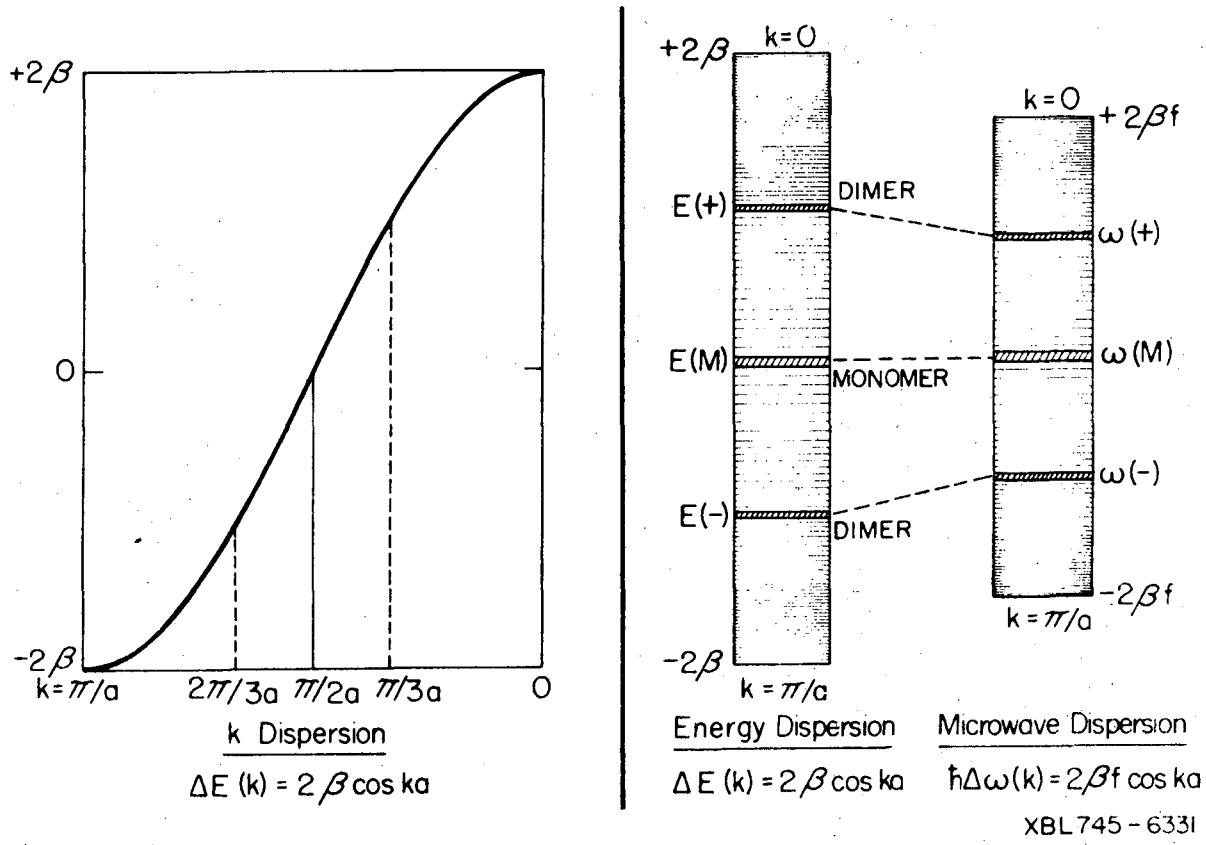

Fig. 12

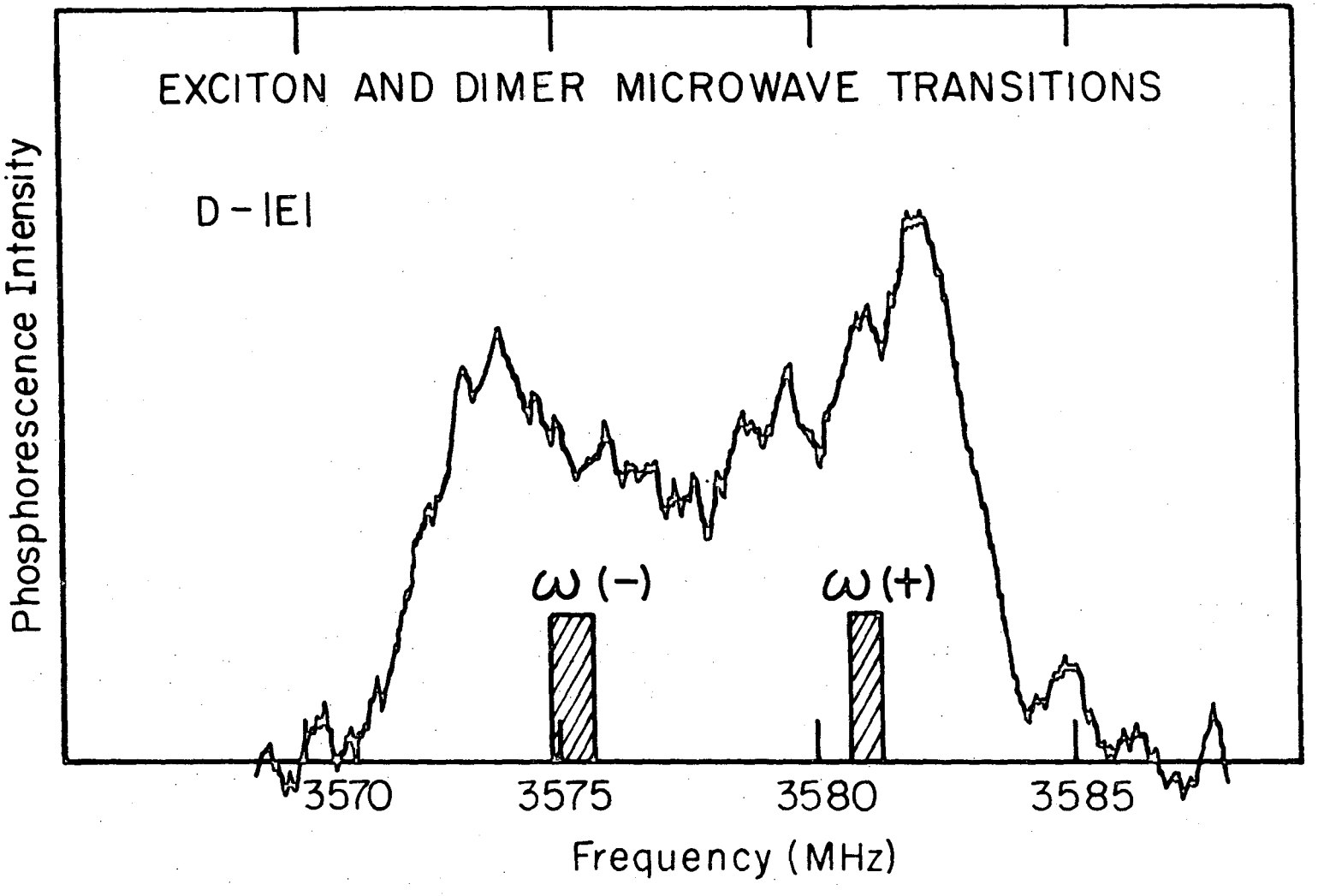

XBL745-6327

Fig. 13

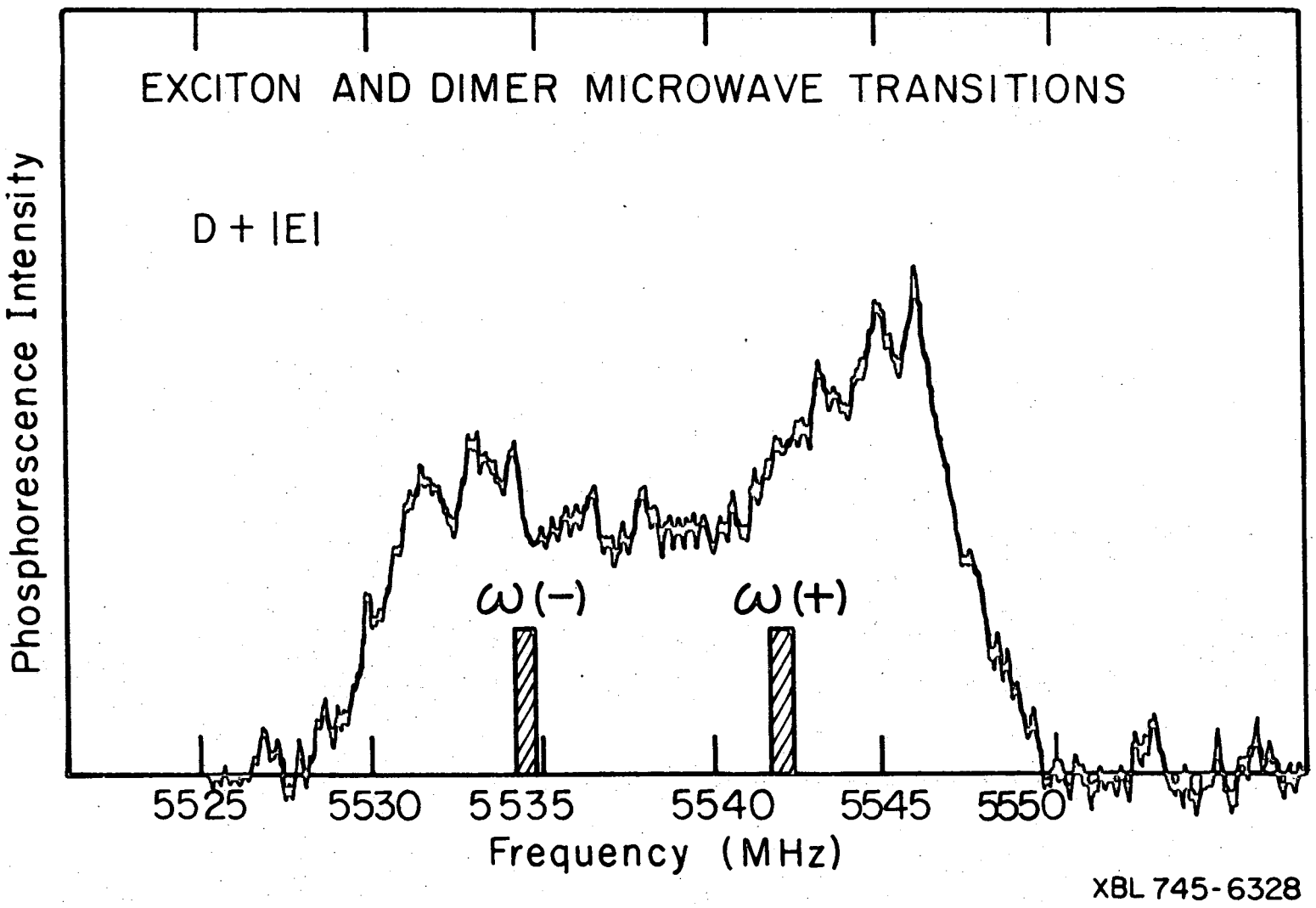
EXCITON AND DIMER MICROWAVE TRANSITIONS
D + |E|
Phosphorescence Intensity
ω(−)
ω(+)
5525
5530
5535
5540
5545
5550
Frequency (MHz)
XBL 745-6328

Fig. 14

TECHNICAL INFORMATION DIVISION
LAWRENCE BERKELEY LABORATORY
UNIVERSITY OF CALIFORNIA
BERKELEY, CALIFORNIA 94720